IEEE Access
Multidisciplinary | Rapid Review | Open Access Journal

Received November 30, 2019, accepted December 18, 2019, date of publication January 6, 2020, date of current version January 15, 2020.

Digital Object Identifier 10.1109/ACCESS.2020.2964528

Data Fusion by a Supervised Learning Method for Orientation Estimation Using Multi-Sensor Configuration Under Conditions of Magnetic Distortion and Shock Impact

HUAN LIU[1], ROMAN J. SHOR[2], AND SIMON S. PARK[3]
[1]Department of Geomatics Engineering, University of Calgary, Calgary AB T2N 1N4, Canada
[2]Department of Chemical and Petroleum Engineering, University of Calgary, Calgary AB T2N 1N4, Canada
[3]Department of Mechanical and Manufacturing Engineering, University of Calgary, Calgary AB T2N 1N4, Canada

Corresponding author: Simon S. Park (simon.park@ucalgary.ca)

This work was supported in part by the Alberta Innovates, Alberta, Canada, and in part by the Ruby (U of Calgary) through Scholarship.

ABSTRACT Accurate subsurface sensing during directional drilling is critical in the mining and energy extraction industries. One challenge is to measure the azimuth accurately. Azimuth measurements are hindered by magnetic disturbances such as iron debris, especially when magnetometers are used. Moreover, gyroscopes are susceptible to shocks during drilling surveys. To overcome these challenges, we developed a supervised learning filter (SLF) using a multi-sensor configuration (MSC) to accurately estimate the azimuth. The MSC consists of micro-electro-mechanical systems (MEMS) based magnetometers, gyroscopes, and accelerometers into two set of sensors, and the groups are separated by a known distance D to acquire additional rotational information using a dual acceleration difference (DAD) method. Also, D can reduce the negative effect of magnetic disturbances. A Kalman filter (KF) with known a priori noise information removes white noise; however, it is difficult to deal with unknown magnetic and shock disturbances. To reduce the effect of unknown magnetic and shock disturbances, we use the SLF to estimate orientation information. First, the SLF employs an adaptive neuro network fuzzy inference system (ANFIS) to build error models of each sensor; then the SLF calculates the proper weights of the sensors using the error models. Lab-scale experiments are performed on a test rig where the SLF is evaluated using one case with training and verified using two cases without training. The results showed an improvement in azimuth estimation.

INDEX TERMS Supervised learning filter, directional drilling, mwd, anfis, magnetic disturbance robustness, dual acceleration difference, shock disturbance robustness, subsurface sensing, multi-sensor configuration.

I. INTRODUCTION

Extracting mineral and energy deposits from the subsurface requires accurate positioning information for geosteering and wellbore placement. Directional drilling survey tools used in the petroleum industry use subsurface sensing and are of particular note due to the distances drilled and the exceptional harsh operating environment. The sensors used in drilling survey tools must provide proper three dimensional (3D) positional information, i.e., inclination and azimuth, to steer the drill bit to follow the desired well path [1]. The current direction of subsurface sensing research focuses on integrated micro-electro-mechanical system (MEMS) inertial measurement units (IMUs), because they have the advantages of being small and light weight, manufactured at low cost, and require less power [2]. Typical IMUs used in subsurface sensing usually contain accelerometers, gyroscopes, and magnetometers.

Each type of sensor has different limitations for subsurface sensing; for example, magnetometers and gyroscopes suffer from magnetic and shock disturbances, respectively. Sensor fusion is a technique that automatically analyzes and integrates information from different sensors. A multiple sensor fusion system (MSFS) was recently developed to achieve more accurate estimations than a single sensor or information source alone could provide [3]–[5]. Information integration technologies complement and optimize information from

The associate editor coordinating the review of this manuscript and approving it for publication was Mingjun Dai.

different sensors to achieve the most realistic output possible. This approach minimizes the weaknesses of individual sensors, which may otherwise produce poor readings because of disturbances, noises, and other uncertainties [6].

Compared to a single sensor sensing system, an MSFS is more complicated and is often more costly. However, these disadvantages are minimal compared to the advantages [7]. An MSFS improves robustness since different sensor types compensate for each another in harsh conditions. It also yields performance improvements such as noise reduction and improved accuracy. An MSFS, along with redundant data, can provide more information to help obtain a clearer result [8].

An IMU utilizes a self-contained navigation technique in which measurements are provided by onboard-gyroscopes, magnetometers, and accelerometers. The IMU utilizes these three types of signals to estimate the orientations and positions of an object. Combined with other sensors, such as global positioning systems (GPS), cameras, radar, laser, and others, IMUs may be broadly applied in many applications including dead reckoning, indoor navigation, and measurement while drilling (MWD). MWD systems are typically used to provide the real-time position and orientation of the bottom hole assembly (BHA) during drilling [9]. Current MWD systems are based on magnetic surveying technology [10] where the magnetic surveying part of the MWD system is a special non-magnetic drill collar housing with accelerometers and magnetometers [11]. During MWD operations, two orientation angles are recorded: i) azimuth, the angle on the horizontal plane away from magnetic north and ii) inclination, the angle on the vertical plane away from vertical.

Data from accelerometers and magnetometers are typically used to determine orientation angles. In some tools, gyroscopes are employed to improve the low signal to noise ratios (SNR) of accelerometers and magnetometers [12]. A hybrid multi-sensor system that combines a magnetometer with a gyroscope may increase the accuracy of the azimuth measurement since a gyroscope's signal has low SNR and is robust against magnetic disturbances. Combing these two sensors with a Kalman filter (KF) removes the noise inherent in magnetic signals and reduces the integration drift caused by the direct current (DC) component of gyroscope signals [13].

Gyroscope data can also update the headings. Therefore, in the presence of magnetic disturbances, a gyroscope is employed to correct the heading errors [14], [15]. However, there are several problems associated with gyroscope compensation. Unlike typical sensing activities at the surface, such as indoor or outdoor vehicle movement detection, motion in the subsurface is much slower – on the order of meters per minute to meters per hour, which means a magnetometer may be exposed to ferromagnetic objects for an extended period of time; therefore, the drift caused by the DC component of gyroscope data may affect the accuracy of the orientation estimation [16]. Also, shocks could cause large drifts in the integral calculation of gyroscope data because gyroscopes are significantly affected by shocks.

During MWD operations, the drill string may be stationary (while not drilling) or rotating (while drilling). In addition to drift in the integral calculation of gyroscopic data, gyroscopes' application for rapidly rotating objects of large accelerations are challenging [17], [18] since each gyroscope is designed for a particular maximum angular velocity, particularly for MEMS gyroscopes [19]. MEMS gyroscopes used in this study are strongly affected by large rotational velocities (sometimes thousands of degrees/s) during the drilling process because a typical MEMS gyroscope is limited to only hundreds of degree/s [20], [21]. Also, MEMS gyroscopes are subjected to various shock impacts [22]. Typical MWD tools currently used in industry favor accelerometers [23], but gyroscopes are often found in tools used for continuous drilling survey applications [24]. Non-strapdown based gyroscopes that may be more robust to the downhole environment are available (for example fiber-optic coils); however, current technologies are not economically viable [25].

Therefore, using redundant accelerometers to obtain rotation information is becoming popular [26], [27]. Without the assistance of a gyroscope, the minimum number of accelerometers required to extract 3D rotational information is six [28]. Thus, by using two IMUs, each with three accelerometers on the x, y, and z axes allows for rotational information to be obtained with only accelerometers.

The objective of this research is to enhance the accuracy of continuous wellbore surveys by using two redundant sets of IMUs to reduce the affect of magnetic and shock disturbances. To achieve this objective, we first propose a sensor configuration utilizing dual IMUs separated by a fixed known distance, D to reduce influence of magnetic disturbances; when one magnetometer is affected by the magnetic disturbances, the other magnetometer is unaffected since the influence of the interference is reduced as an inverse power function of D [40], [41]. This configuration also provides redundant azimuth angles using the dual accelerometer difference (DAD) method for cases where gyroscopes are absent. Based on the sensor configuration (hardware design), we then developed a supervised learning filter (SLF) to reduce the effect of magnetic and shock disturbances. For the SLF, an adaptive neuro fuzzy inference system (ANFIS) is employed to build the error models of different orientation angles obtained from accelerometers, gyroscopes, and magnetometers. Weights are calculated using the outputs of these error models for each sensor, and these weights show the accuracy of each sensor in an applied environment.

II. EXPERIMENTAL SETUP

A. TEST RIG

The proposed sensor fusion method was tested using a lab-scale test rig. The rig consisted of a two-axis turntable riding on a single linear stage and three encoders located on three DC drive motors, which were used to track the movements of the system. This test system allowed for the dynamic testing

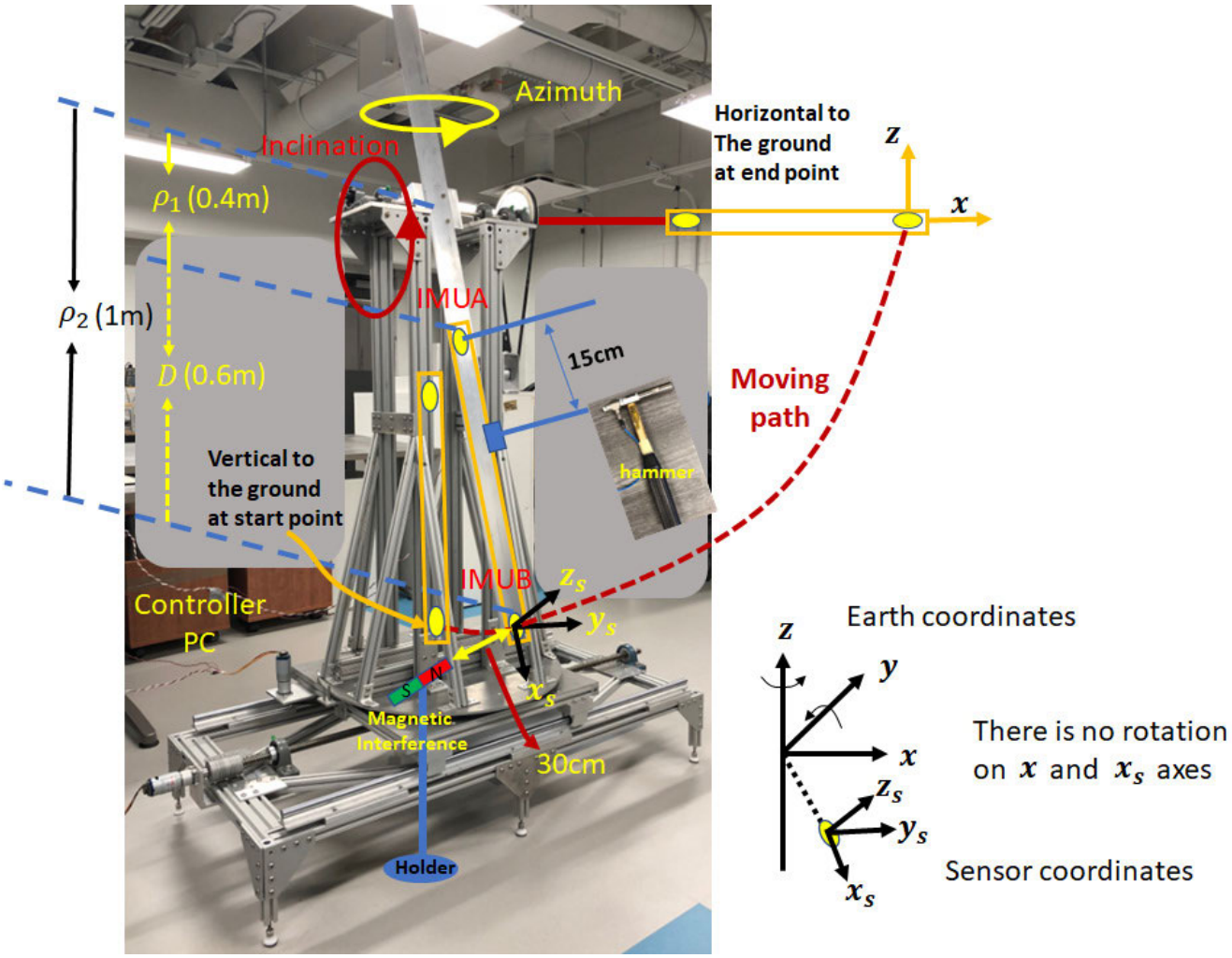

FIGURE 1. Lab-scale test rig: this test system allows for the dynamic testing of sensor states such as inclination and azimuth.

of sensor states such as inclination and azimuth (Figure 1). Rotational information of the various motors was recorded by a set of encoders transmitted to a PC controller. Desired motion paths and speeds were programed through the PC. The orientation angles, such as pitch and azimuth, could be set, and recorded data were saved as a time series.

B. SENSOR SETUP AND TRAJECTORY PLAN

The sensor setup contained dual IMUs, each of which had triaxial gyroscopes (×3), accelerometers (×3), and magnetometers (×3) located on the x, y, and z axes, and data were sampled at 205Hz. The IMUs were separated by 0.6 m; IMU_A was located 0.4 m from the center of rotation and IMU_B was located at 1.0 m. They were assumed to be mounted on a rigid body. The reference azimuth was obtained from the encoders on the motors. Sensor noise was classified as constant bias, calibration errors (scale factors, alignments and linearities), white noise, and pink noise ($1/f$) [29], [30]. Constant bias and calibration errors were removed by the calibration methods [31]–[34].

Magnetometers also suffered from pink noise [35], [36], but it was not quantified by the manufacturer. Noise levels are shown in Table 1.

The test rig was hit three times, 0.4 seconds apart using an impact hammer (PCB 208. A03) to simulate shocks. Magnetic disturbances were imitated using a permanent magnet (4.2×10^5 nT with a 50 mm distance) placed temporarily near one of the IMUs. Planned trajectories were implemented using the test rig. The coordinate frame was anchored at the IMUs as shown in Figure 2. The experimental events timeline is shown in Table 2. From 0 to 11 seconds is Rest1; from 11 to 19 seconds is Rotation1; from 13 to 16 seconds is the first magnetic disturbance; from 13.6 to 15 seconds is the shock disturbance; from 19 to 40 seconds is Rest2; from 40 to 48 seconds is Rotation2; from 43 to 46 seconds is the second magnetic disturbance; from 48 to 59 is the last rest.

III. METHODOLOGY

The orientation angles may be obtained using magnetometers (azimuth), accelerometers (inclination and tool face),

TABLE 1. IMU noise specification [38].

		IMU		
	Parameter	Conditions	Value	Unit
Gyroscope	Angular Random Walk	1σ	0.66	$°/\sqrt{hr}$
	In-Run Bias Stability	1σ	14.5	$°/hr$
	Output Noise	RMS	0.27	$°/sec$
Accelerometer	Velocity Random Walk	1σ	0.11	$°/\sqrt{hr}$
	In-Run Bias Stability	1σ	0.25	mg
	Output Noise	RMS	5.1	mg
Magnetometer	Output Noise	RMS	2.4	$mgauss$

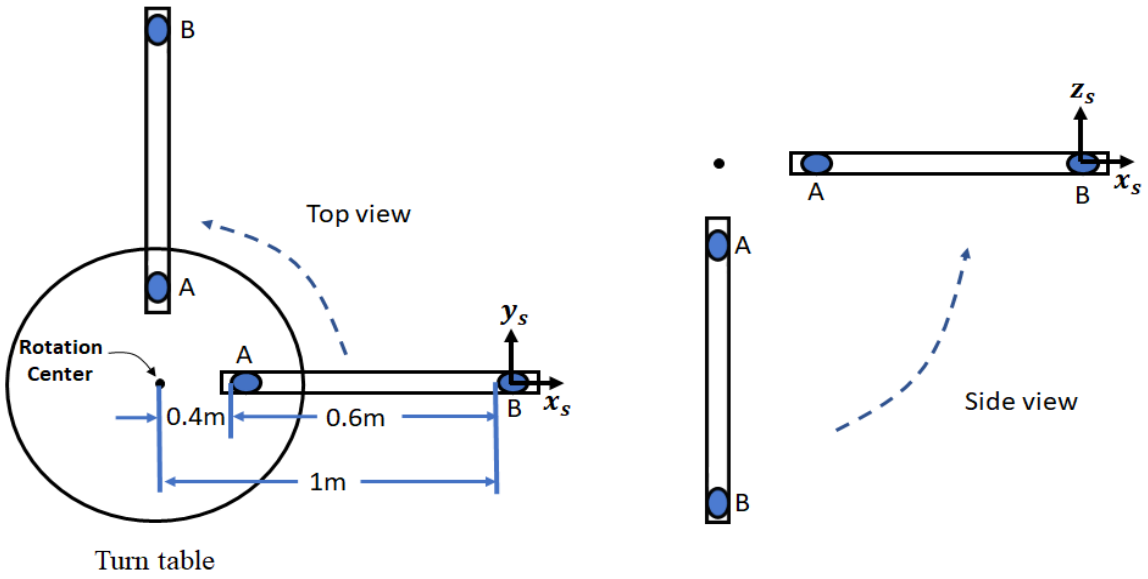

FIGURE 2. Planned trajectories were implemented using the test rig.

and gyroscopes (all angles). However, an accurate azimuth is relatively difficult to obtain due to magnetic and shock disturbances. To reduce the effect of magnetic and shock disturbances, the proposed SLF first collects azimuth angle data sets from magnetometers, gyroscopes, and accelerometers; next, SLF employs ANFIS to build error models of each sensor; finally, SLF compares the errors from the ANFIS models to calculate the weights of the sensors. In this section, we introduce how to obtain rotational information from the DAD method in section A; then, we explain the design details of the SLF in section B.

A. AZIMUTH ANGLES OBTAINED FROM DUAL ACCELERATION DIFFERENCE (DAD) METHOD

1) DAD AZIMUTH

Gyroscopes are good at obtaining angular velocities under dynamic situations. However, the maximum angular speed measurement limitation, which is caused by the internal structure of a gyroscope, reduces industry applications [20], [21]. Also, the detrimental effect of shock impacts on a gyroscope is an other limitation [22]. Using dual tri-axis accelerometer sets separated by a known distance to find the angular velocity estimations [37], we can increase redundant orientation estimation. As shown in Figure 3, the acceleration magnitude (a_p) of a moving point is calculated as follows:

$$a_p = \sqrt{\ddot{x}^2 + \ddot{y}^2 + \ddot{z}^2} = \sqrt{a_N^2 + a_T^2} \tag{1}$$

where $\ddot{x}, \ddot{y}, \ddot{z}$ are the particle accelerations on the x, y, and z axes respectively, a_N is normal acceleration, and a_T is tangential acceleration. The difference between the two normal accelerations is determined as follows:

$$a_{N_B} - a_{N_A} = (\rho_2 - \rho_1)\left(\dot{\theta}_z^2 + \dot{\theta}_y^2\right) = D\left(\dot{\theta}_z^2 + \dot{\theta}_y^2\right) \tag{2}$$

TABLE 2. Experimental events time-line. From 0 to 11 seconds is Rest1; from 11 to 19 seconds is Rotation1; from 13 to 16 seconds is the first magnetic disturbance; from 13.6 to 15 seconds is the shock disturbance; from 19 to 40 seconds is Rest2; from 40 to 48 seconds is Rotation2; from 43 to 46 seconds is the second magnetic disturbance; from 48 to 59 is the last rest.

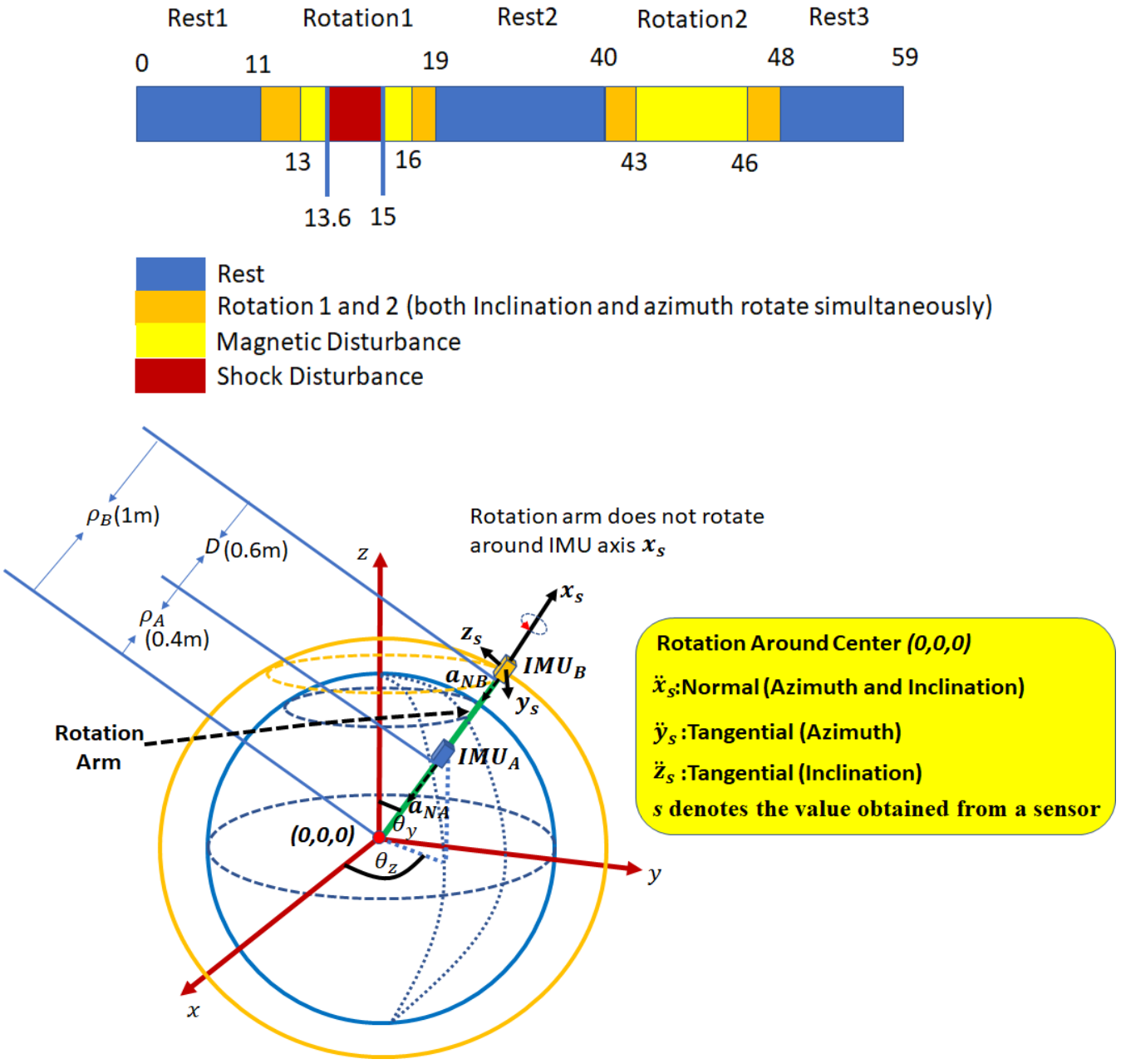

FIGURE 3. Spherical coordinates for two redundant accelerometers. These two accelerometers are mounted on a rigid body and separated by a constant distance D.

The x axis of the IMU is oriented along the rotation radius (normal direction, as shown in x_s of sensor in Figure 3); the y and z axes of the IMU are along the tangential direction of the rotation (y_s, z_s axes in Figure 3); and the rotation center of the IMU is set at (0,0,0); however, the rotation arm does not rotate around the IMU x_s axis due to our test rig design.

Based on the configuration of the sensor arrays, the normal components of the accelerations of Equation 2 may be measured by the x_s axes of the sensors. Therefore, the normal accelerations a_{NA} and a_{NB} measured by IMU_A and IMU_B are denoted as $\ddot{x}_{s_A}$ and $\ddot{x}_{s_B}$, respectively. The difference between these two normal elements of the acceleration can be used to calculate the square root sum of the roation speeds of the inclination and azimuth (Equation 3).

$$\dot{\theta}_N = \sqrt{\dot{\theta}_z^2 + \dot{\theta}_y^2} = \sqrt{\left|\ddot{x}_{sc_B} - \ddot{x}_{sc_A}\right| / D} \tag{3}$$

The earth's gravity is embedded in the two sets of measurement from the IMUs (DC coupled), and the measurements are subtracted ($|\ddot{x}_{scB} - \ddot{x}_{scA}|$). Therefore, no gravity effect to the final calculation of the equation. However, the accelerometer measurements $\ddot{x}_{sA}$ and $\ddot{x}_{sB}$ which still need to be corrected [37], show that Equation (3) works well for higher rotation rates (>140deg/s), but it does not work well for lower rotation rates (<140deg/s) because the accelerometers do not measure proper dynamic acceleration values accurately. In this paper, we extend Equation (3) to include lower rotations using a correction method, shown in next section. Here, the s denotes the acceleration value from an IMU, and sc means the value is corrected.

$$\dot{\theta}_{zDAD} = \vartheta_{Azi} * \dot{\theta}_N \tag{4}$$

$$\vartheta_{Azi} = \frac{\dot{\theta}_z}{\sqrt{\dot{\theta}_z^2 + \dot{\theta}_y^2}} \tag{5}$$

As $\dot{\theta}_{normal}$ in Equation (3) includes the components of inclination and azimuth angular velocities and is always positive, it can not be used directly. As shown in Equations (4) and (5), ratio factor ϑ_{Azi} identifies the proper percentage of azimuth, and the factor provides corrected rotation directions (positive and negative signs of the calculated rotational angular speeds). This ratio factor is obtained from the integration of the tangential accelerations [37] or derived from azimuth (magnetometer) and inclination (gravity) angular values.

2) ACCELERATION CORRECTION

The maximum rotational speed of our test rig is lower than 140deg/s, and Equation (3) does not work properly when rotation speeds are <140deg/s. Therefore, our accelerometers do not accurately determine proper dynamic accelerations.

To deal with this problem, we use ANFIS to correct the dynamic accelerations. As shown in Figure 2, two IMUs rotate in the azimuth and inclination directions. During the rotation, the two IMUs are located on the same side of the rotation center. According to Equation (3), the difference value of the normal accelerations is calculated as follows:

$$|\ddot{x}_{sB} - \ddot{x}_{sA}| = D\left(\dot{\theta}_z^2 + \dot{\theta}_y^2\right) \tag{6}$$

where, D (0.6 m) is the distance between the two sets of accelerometers, and $\dot{\theta}_y$ and $\dot{\theta}_z$ are rotational angular speeds, obtained from other sensors such as gyroscopes or encoders (through converting calculations). If the rotation is slow, Equation (6) contains an error because the accelerometers may not sense small dynamic accelerations. The error is shown as follows:

$$Err_{\ddot{x}1} = |\ddot{x}_{sB} - \ddot{x}_{sA}| - D\left(\dot{\theta}_y^2 + \dot{\theta}_z^2\right) \tag{7}$$

Also,

$$\begin{aligned} |\ddot{x}_{sB} + \ddot{x}_{sA}| &= (2R_A + D)\left(\dot{\theta}_y^2 + \dot{\theta}_z^2\right) \\ &= (2R_B - D)\left(\dot{\theta}_y^2 + \dot{\theta}_z^2\right) \end{aligned} \tag{8}$$

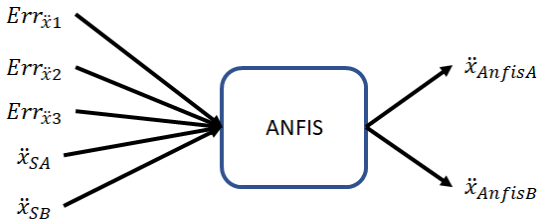

FIGURE 4. Dynamic acceleration compensation using ANFIS. The inputs are low rotation error ($Err_{\ddot{x}_1}$,$Err_{\ddot{x}_2}$,$Err_{\ddot{x}_3}$), accelerometer readings ($\ddot{x}_{s_A}$, $\ddot{x}_{s_B}$), and the outputs are two compensated centripetal accelerations.

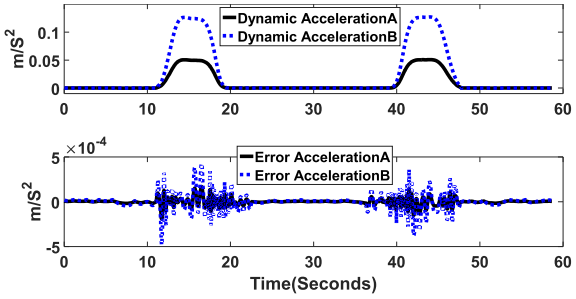

FIGURE 5. The top sub-plot shows the compensated centripetal accelerations ($\ddot{x}_{sc_A}$, $\ddot{x}_{sc_B}$); the bottom sub-plot shows the errors of the two compensated accelerations.

Therefore,

$$Err_{\ddot{x}2} = |\ddot{x}_{s_B} + \ddot{x}_{s_A}| - (2R_A + D)\left(\dot{\theta}_{sy}^2 + \dot{\theta}_{sz}^2\right) \tag{9}$$

$$Err_{\ddot{x}3} = |\ddot{x}_{SB} + \ddot{x}_{SA}| - (2R_B - D)\left(\dot{\theta}_{sy}^2 + \dot{\theta}_{sz}^2\right) \tag{10}$$

Based on the errors $Err_{\ddot{x}_1}$, $Err_{\ddot{x}_2}$, and $Err_{\ddot{x}_3}$ and the accelerometer readings $\ddot{x}_{s_B}, \ddot{x}_{s_A}$, ANFIS is applied to correct the normal accelerations as shown in Figure 4.

Figure 5 shows the corrected normal accelerations A & B (top sub-plot), after the proposed ANFIS correction, the errors are small after the compensation as shown in the bottom sub-plot. The AME values of the compensated accelerations are around $\mathbf{0.00019}\boldsymbol{m/s^2}$ (A) and $\mathbf{0.00048}\boldsymbol{m/s^2}$ (B).

B. SLF FOR OBTAINING AZIMUTH INFORMATION

Identifying when measurements have low accuracy, as during a shock event or while passing a magnetic disturbance, is paramount to effective sensor fusion. For example, as one of the redundant IMUs passes a magnetic disturbance, the magnetometer is adversely affected, but the gyroscope remains unaffected.

By estimating the azimuth angle using the weighted information obtained from different sensors and methods, we can then find a weighted average of different azimuth angles, which can provide an appropriate estimation of azimuth despite magnetic disturbances. To determine the proper weights of each azimuth angle, a fuzzy inference system (FIS) is employed. In this paper, we propose a special process of ANFIS to tune the membership functions and design the

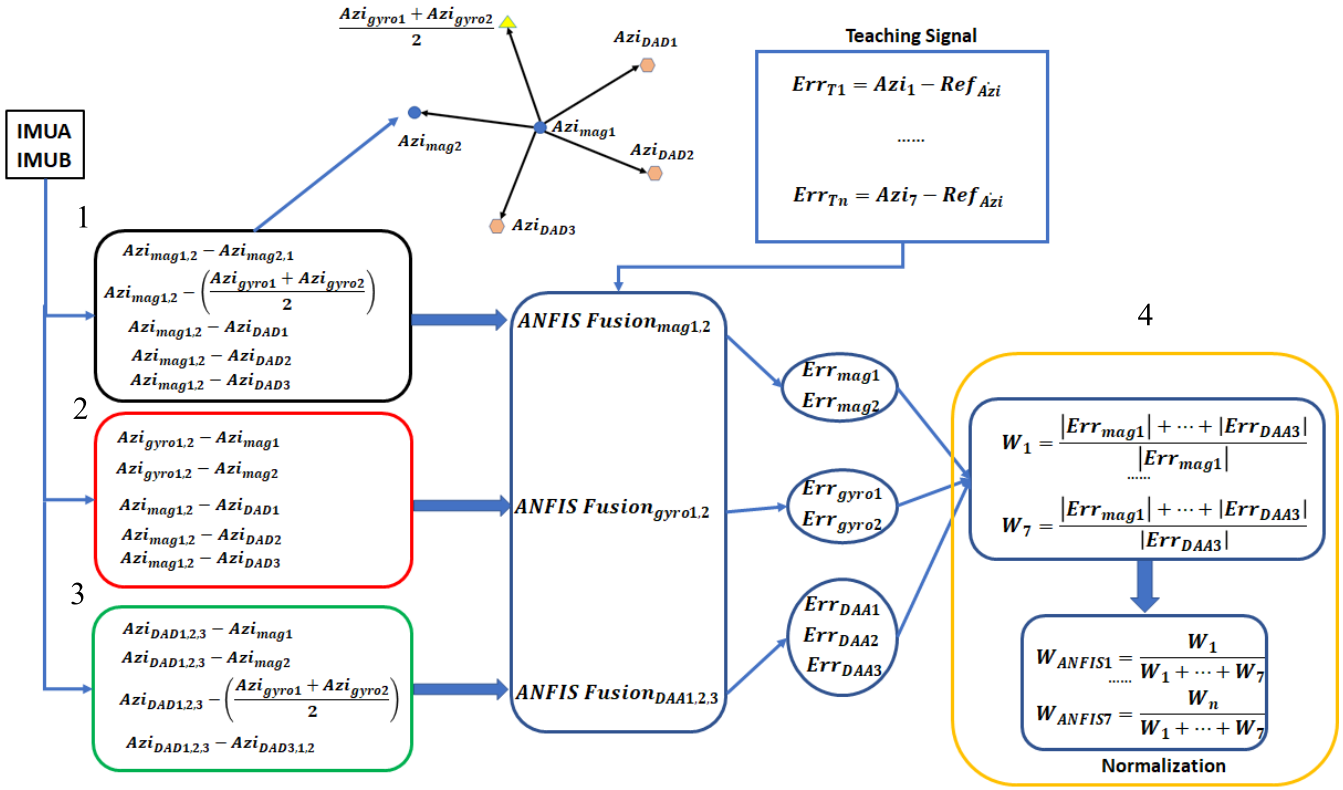

FIGURE 6. The structure of the ANFIS, after training by the teaching signal ANFIS is used to build error models of each sensor; then the outputs of ANFIS are used to determine the weights of the sensors.

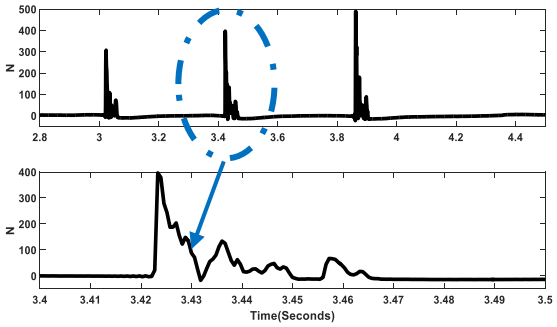

FIGURE 7. Shock forces measured from the shock test; 3 hits with a time interval around 0.4 seconds. The force peak values of the 3 hits are around 300N, 400N, and 500N.

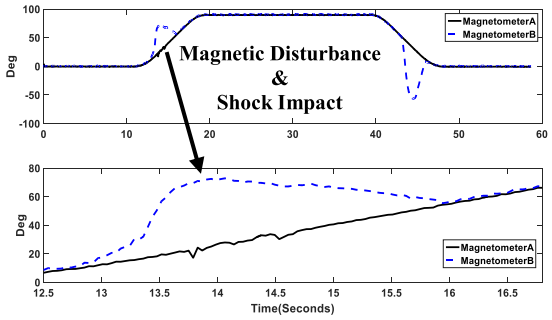

FIGURE 8. Azimuth angles of the two magnetometers from lab-scale tests; magnetometer$_B$ is influenced twice by magnetic disturbances; both magnetometers (A & B) suffer from shock impacts.

precise fuzzy rules to improve final efficiency and to build the error model of each sensor. Sensor values are used as the inputs of the ANFIS model to output the error of each sensor. Based on the magnitudes of these errors, the weight of each sensor can be computed.

1) ERROR TEACHING SIGNAL

To obtain teaching signals for error model training, we first computed various azimuth angles using measurements obtained from magnetometers, gyroscopes, and the DAD method (accelerometers); then, we compared the computed angles with a reference angle to calculate the errors. For our lab-scale evaluation, we used signals from the encoder of the rotation motor as a reference.

2) SLF LOGIC

The first function of this design is to estimate the magnetometer errors caused by the interferences to reduce the effect of magnetic disturbances. We have two azimuth angles from the magnetometers (Azi_{mag1}, Azi_{mag2}), two azimuth angles from gyroscope signal integrations (Azi_{gyro1}, Azi_{gyro2}), and three azimuth angles from the accelerometers (Azi_{tangen}, $Azi_{centri1}$, $Azi_{centri2}$) using the DAD method. There are three clusters of inputs identified with different color blocks (1: black; 2: red; 3: green). For each cluster, one kind of sensor is used as

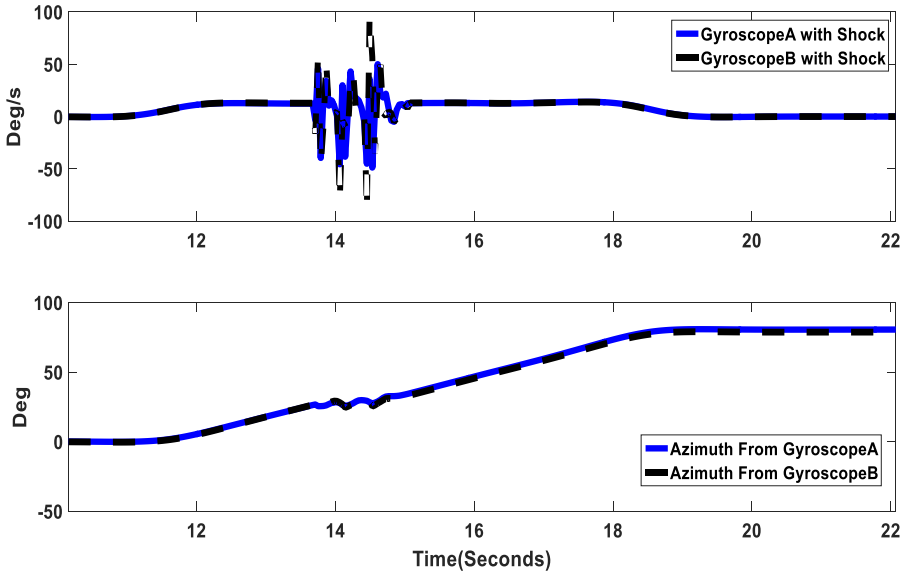

FIGURE 9. Gyroscope data from a shock impact: the shock impact causes drift (about 10 degrees) in the angle integration (azimuth) as shown in the bottom subplot.

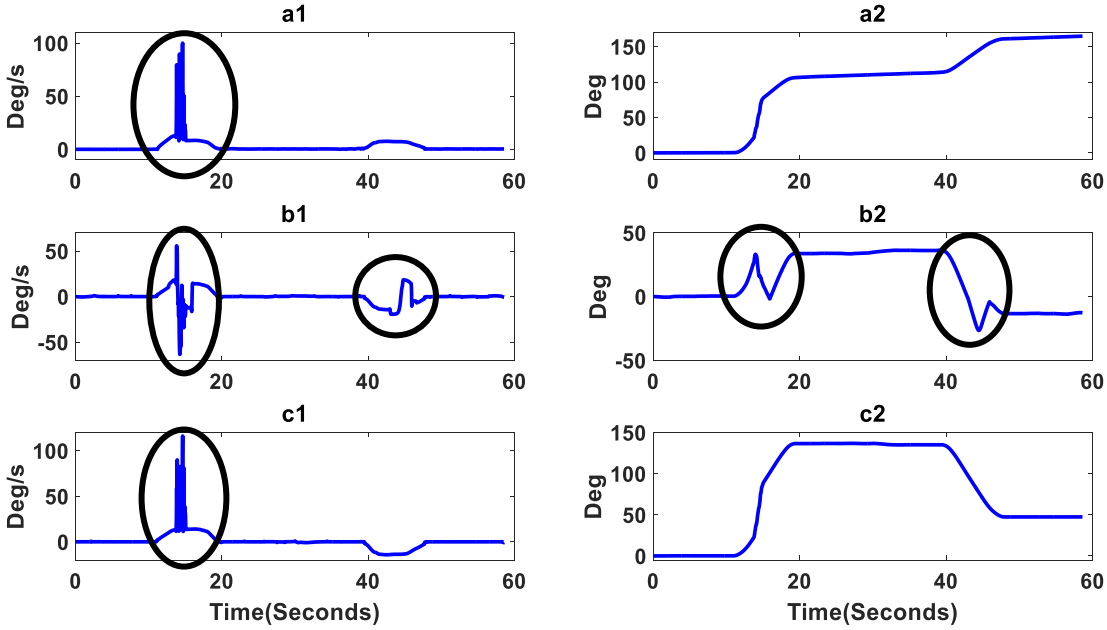

FIGURE 10. Data from the differential method of two accelerometers under a shock impact; the shock causes drift in the azimuth angle integration.

a reference to which the other sensors are compared; The errors are then used as inputs for ANFIS to build the error models (black center: magnetometers; red center: gyroscopes; green center: dual accelerometers). For example, as shown in the black block of Figure 6, each azimuth angle from a magnetometer is compared with the azimuth angles from the other magnetometer, gyroscopes, and accelerometers. The relationship between these relative differences and the sensor error can be built with ANFIS as shown in Figure 4, which means the error model of each sensor can be estimated using the relative differences between this sensor and other sensors. After comparising the errors of all sensors, the weights of these sensors are obtained.

For example, if IMU_A is affected by a magnetic disturbance, but IMU_B is not, the magnetometer in IMU_A will not agree with the measurements from IMU_A, while all measurements from IMU_B will be in agreement. In the event of a shock event, the gyroscopes in both IMU_A and IMU_B will be affected, but disagreement between sensor measurements can still be used to compute the errors in the signals because

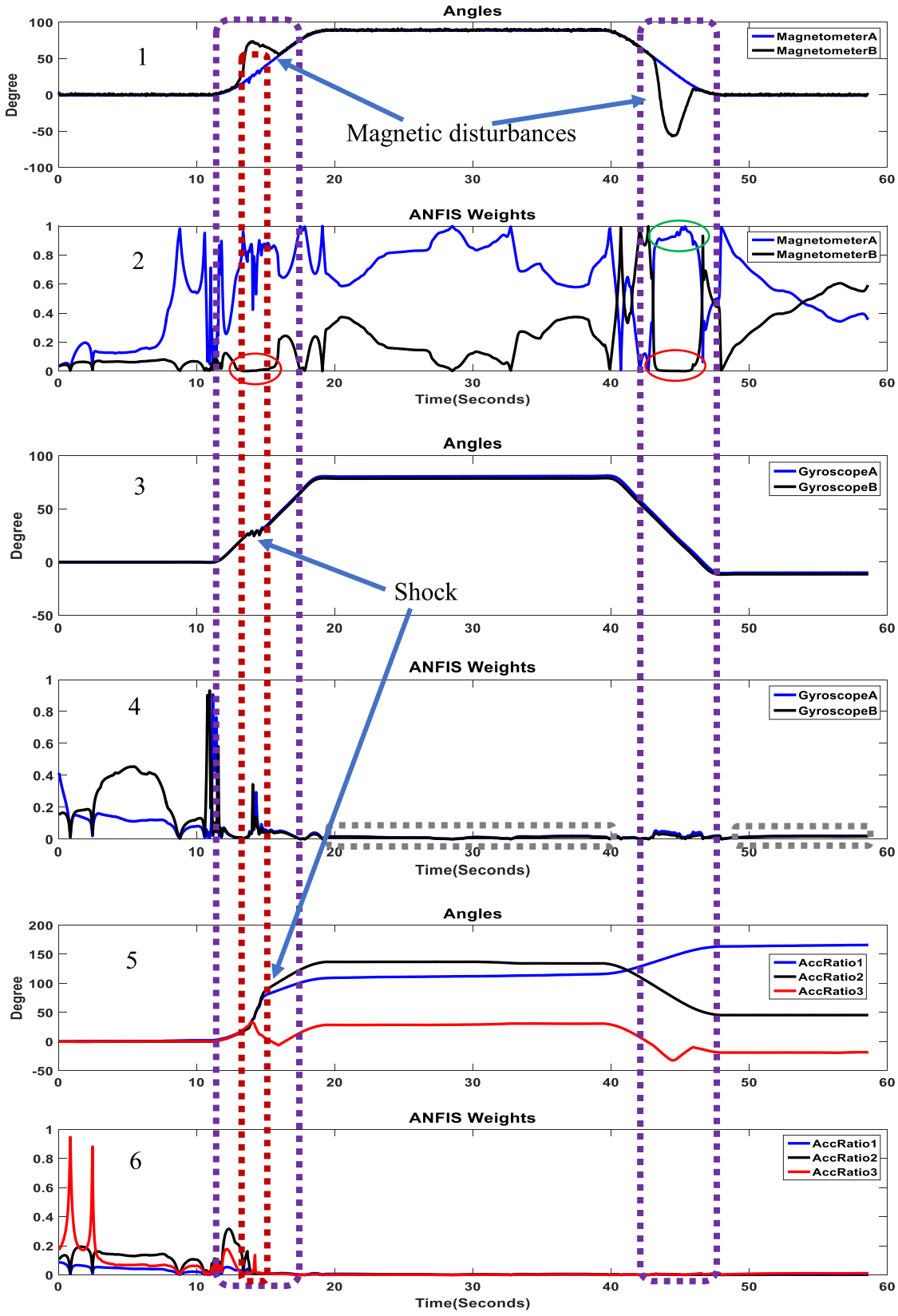

FIGURE 11. Sensor weights calculated by ANFIS; the blocked off parts show that, when subjected to magnetic disturbances and shocks, the weights of the sensors are tuned automatically.

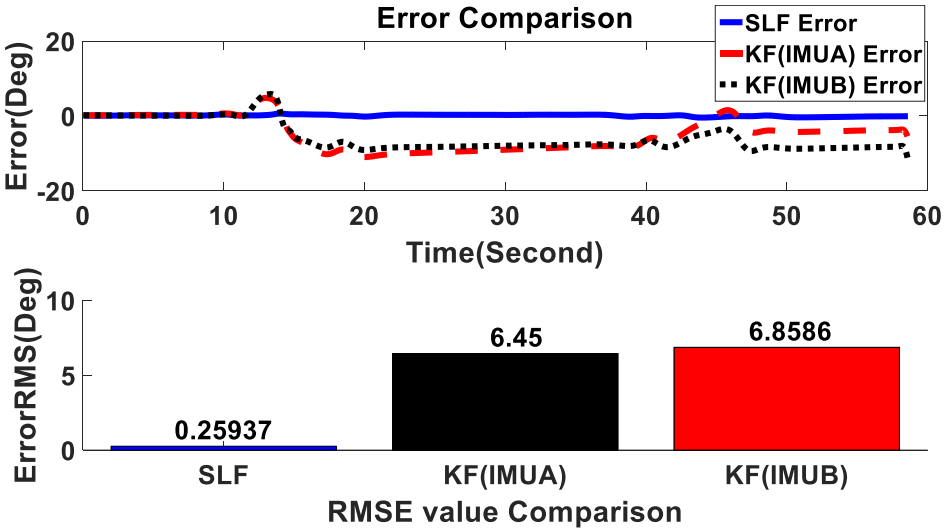

FIGURE 12. The proposed ANFIS method compared with a traditional KF; the covariance matrices are computed based on the standard deviation values of the first 1000 measurements from the gyroscope and magnetometer.

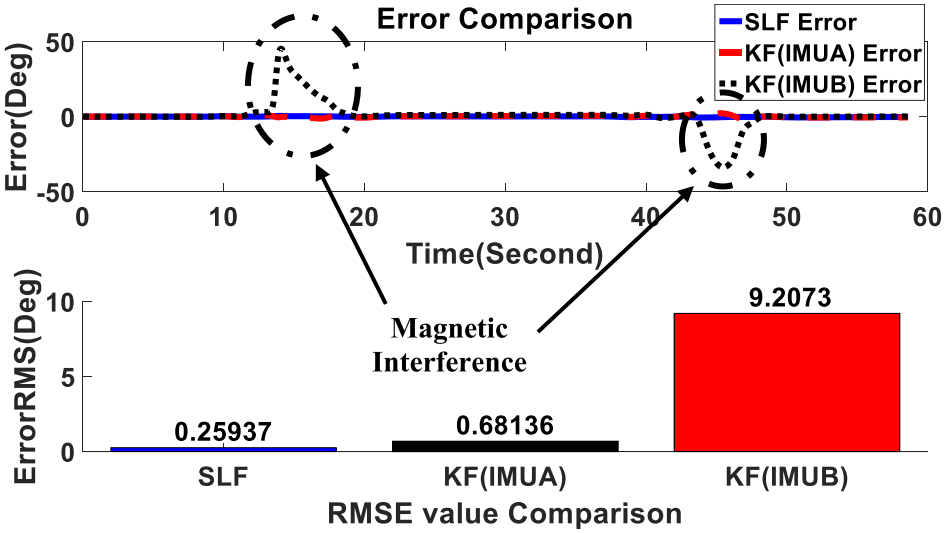

FIGURE 13. The proposed ANFIS method compared with a traditional KF; the covariance matrix Q is computed based on the assumption that the gyroscope disturbances from the shock are known.

the magnetometers are less affected by shocks, and therefore, will have more accurate measurements [39]. Calculation of the weights of $W_{ANFIS1} \ldots W_{ANFIS7}$ based on the different azimuth error values is shown in Figure 6 (4: orange block); the ratio of one error to the sum total error is the weight that denotes how accurate the sensor is. After normalization, these weights are used for the final azimuth output.

IV. LAB-SCALE EVALUATION AND RESULTS DISCUSSION

We present two case studies to evaluate the performance of the proposed muti-sensor configuration and the fusion method. For the first case study, we applied a magnetic disturbance to one magnetometer. The other magnetometer was unaffected because it was placed a distance D away from the first magnetometer [40], [41].Additionally, the gyroscopes and acceleroemters were subjected to shocks

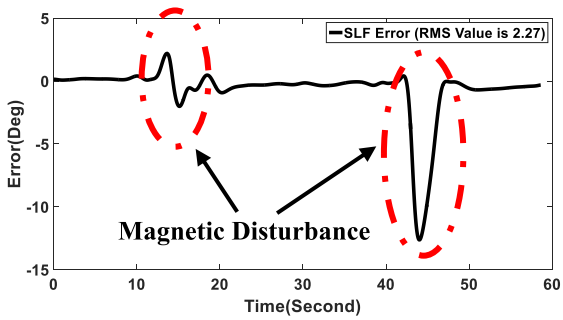

FIGURE 14. The proposed ANFIS method; if all sensors are not accurate, the performance of the ANFIS method is reduced.

since both IMUs were mounted on a single rigid body. For the second case study, both magnetometers were affected by the same level of magnetic disturbances simultaneously.

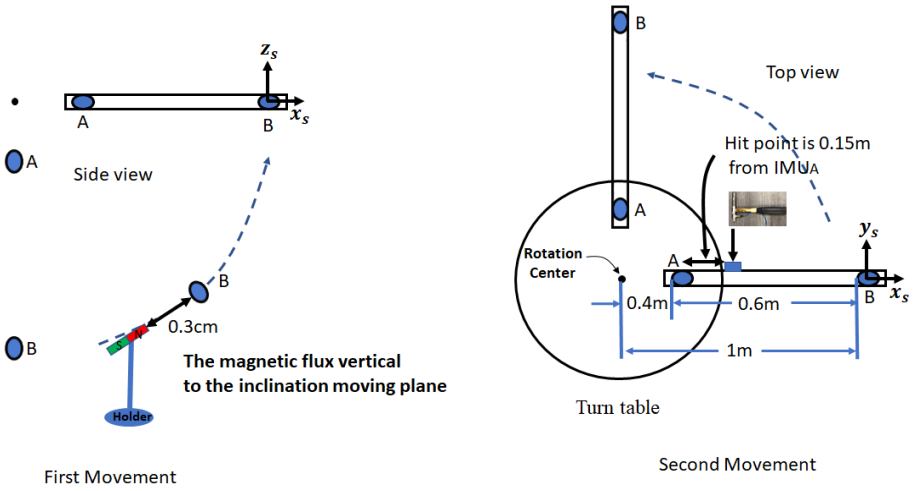

FIGURE 15. Rotational plan of verification case 1.

Also, as in the first case study, all sensors were disturbed by shocks.

Furthermore, we investigated the sensitivities of the proposed SLF.

A. MAGNETIC INTERFERENCE AND SHOCK IMPACT (CASE STUDY 1)

Figure 7 shows the shock forces measured by a shock hammer sensor during a shock test (3 direct impacts to the rotation arm at 15 cm from IMU_A and 45 cm from IMU_B).

Figure 8 shows the data from the two magnetometers: the azimuth angle from $magnetometer_A$ is blue, and the azimuth angle from $magnetometer_B$ is black. $Magnetometer_B$ was affected twice by the simulated magnetic interferences, while $magnetometer_A$ remained unaffected by both interferences. The lower subplot of Figure 8 shows the magnetometers are slightly affected by the shocks (the noise data are measured from the shock experiment, Figure 7). The data from $magnetometer_A$ clearly shows the effect of the shocks, but for $magnetometer_B$, the effect of the shocks is unclear because $magnetometer_B$ suffered from both the shocks and the magnetic disturbance at the same time.

Figure 9 shows the output results of the impact of the shocks on the gyroscopes. The disturbance data were obtained from the same shock test. The bottom plot of Figure 9 shows the integration of the gyroscope signal (angular velocity). The results show that the shock impact caused an angle drift (around 10 degrees) during the integration process.

Figure 10 shows the angular speed from two accelerometers (disturbances were obtained from the same experiment) and their integrations (rotation angles). These results were calculated from Equation (4) with different ratio factors (a_1&a_2 show the ratio factor obtained from the tangential accelerations; b_1&b_2 show the ratio factor calculated from the magnetometer azimuth and gravity inclination of IMU_B, which is affected by the magnetic interferences; c_1&c_2 show

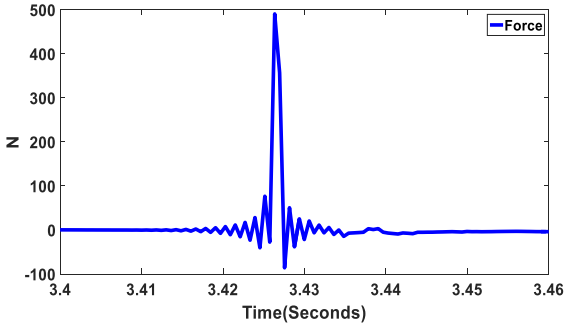

FIGURE 16. Shock force in verification case 1.

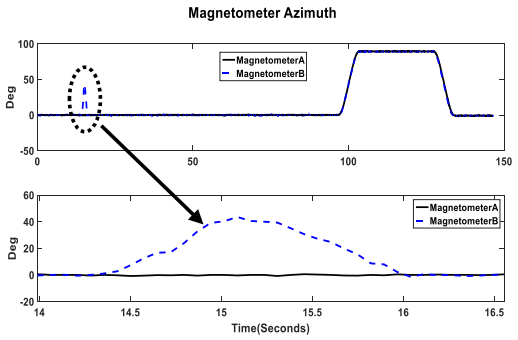

FIGURE 17. The magnetic disturbance in verification case 1.

the factor is from IMU_A, which is not affected by the magnetic interferences). DAD provides redundant azimuth information, but as indicated in the final integrated results (second column of Figure 10), the angles drift due to the shock.

Figure 11 shows the weights calculated by SLF (the SLF method structure is shown in Figure 6). There are seven weights for the seven azimuth angles. They are classified by sensor type with the same time-line. The SLF weights shown in subplot 2 of Figure 11 are for the magnetometers (one magnetometer was affected by magnetic disturbances and the

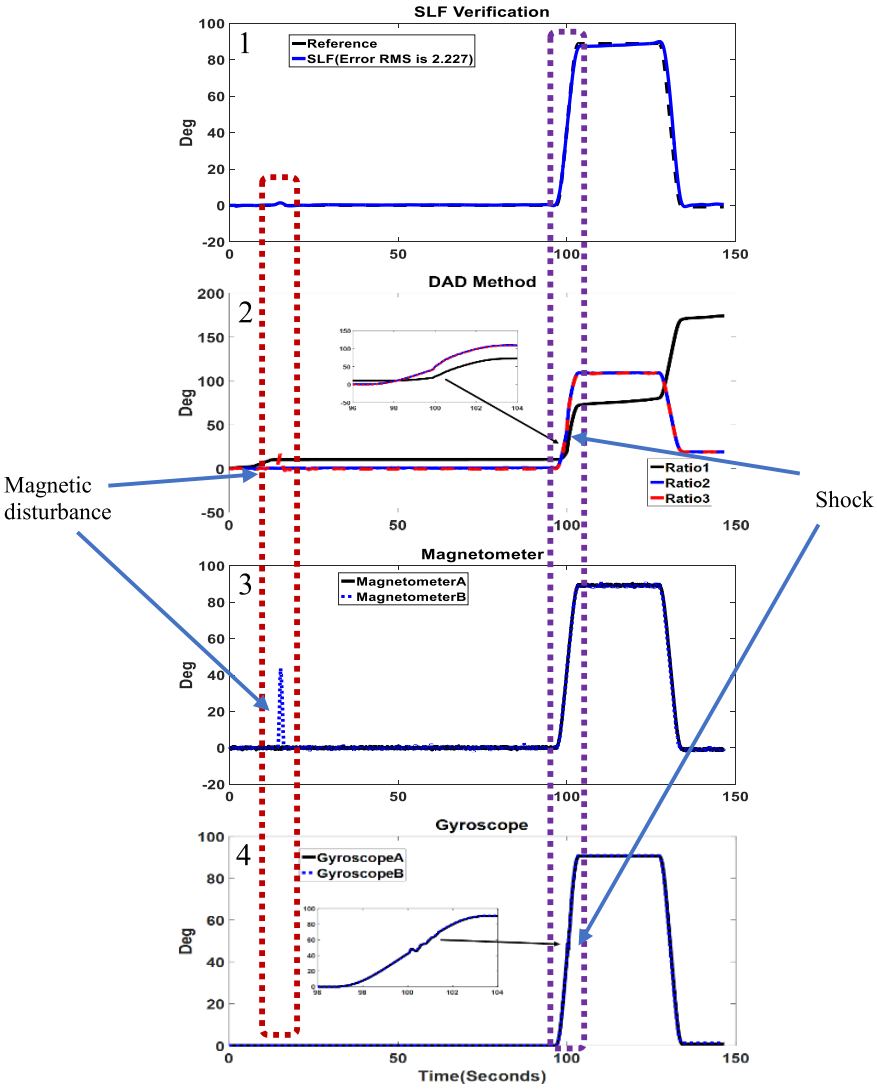

FIGURE 18. SLF performance in verification case 1.

other one was not). As indicated by the purple block, during the magnetic disturbances, the weight of magnetometerB was tuned to zero automatically (red circle in subplot 2); the weight of magnetometer$_A$ was tuned to almost maximum (green circle in subplot 2) because magnetometer$_A$ was not affected by the magnetic disturbances. Moreover, during the shock, the weight of magnetometer$_A$ was reduced (subplot 2, dark red block) because the errors from the other sensors were temporarily reduced by the shock. However, the shock drifted the gyroscope angles about 10 degrees. Therefore, the weights of the gyroscopes were tuned to almost zero (grey blocks in subplot 4 of Figure 11). Finally, the weights of the azimuth angles calculated from 3 different ratio factors were tuned automatically as well (shown in subplot 6 of Figure 11). After the shocks, the magnetometers shared large weights as shown in subplot 2 because the other sensors drifted. Also, the relationship between the two magnetometer weights is inversely proportional: when one reduces, the other one increases. The ratio of the training data and verification data was 5:1.

Figure 12 shows the error between the SLF and a traditional KF (KF of IMU$_A$ with a red dashed line and KF of IMU$_B$ with a black dashed line). We computed the covariance matrices Q & R based on the standard deviation value of the first 1000 measurements from IMU$_A$ and IMU$_B$. The calculated variance values of the covariance matrices Q & R were constants during the computation process of the KFs. The KFs drifted (Figure 12) because of the values of the Q & R matrices; KFs determined that the gyroscopes were more trustworthy than the magnetometers. Therefore, when the gyroscopes drifted because of the shocks, the outputs of the KFs drifted, too. To investigate the influence of the magnetic disturbances, we assumed the gyroscope errors caused by the shocks were known and put them into the Q matrix.

Figure 13 shows that the KF of IMUA is not affected by the shocks because the magnetometer provides accurate

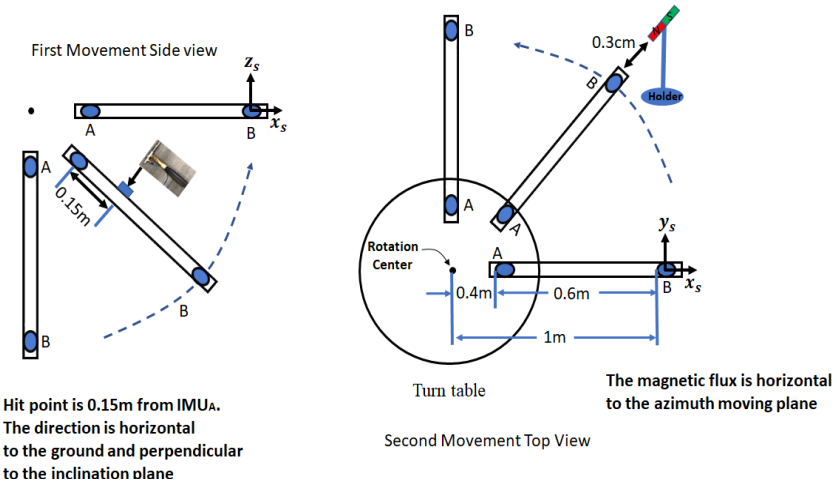

FIGURE 19. Rotational plan of verification case2.

information (magnetometer$_A$ is not affected by magnetic interferences). However, the KF of IMUB shows larger errors than IMUA because the unknown magnetic interferences affected IMUB (the errors caused by the unknown magnetic interferences were not put into the R matrix). The black dashed circles in Figure 13 are the errors in the magnetic disturbance. The absolute maximum error (AME) of SLF is 0.98 degrees; the AME of KF is 11 degrees (Figure 12) and 47 degrees (Figure 13). With training, SLF reduced the effect of magnetic and shock disturbances. The KF performed more poorly compared to SLF.

B. MAGNETIC INTERFERENCE AND SHOCK IMPACT (CASE STUDY 2)

Figure 14 shows the SLF results in the case where all sensors are influenced. The response results of SLF to the disturbances are circled in the figure. If all sensors are influenced by the disturbances, the sensors do not adequately compensate for each other, and the performance of SLF is reduced. To obtain accurate results using SLF, we assume that at least one sensor does not suffer from the disturbances. The gyroscopes and accelerometers cannot avoid the effects of the shocks since they are mounted on a rigid body, but the magnetometers are not sensitive to shocks [39]. Moreover, the distrance D between the two magnetometers reduces the effect of magnetic disturbances. Therefore, SLF performs well if at least one magnetometer is not affected by the disturbances. Also, the rotational information provided by the DAD method requires that both accelerometers are located on the same side of the rotational center as shown in Figure 2. However, the proposed SLF design is based on the supervised learning method; therefore, to investigate the sensitivity of SLF to the disturbances with the training signal, we conducted a sensitivity analysis, presented below.

C. SENSITIVITY ANALYSIS

To determine the sensitivity of the proposed method to different disturbances, we evaluated the method using two additional sets of tests. The new applications were verified without further training. In the case study and the 1st sensitivity verification case, we trained the ANFIS error models using a combined movement (inclination and azimuth move simultaneously) and combined disturbances (magnetic and shock disturbances occurred at the same time). Therefore, we used two single movements to verify the performance of the ANFIS filter. The two single movements include one of inclination and one of azimuth (implemented at different times). Also, the shock and magnetic disturbances were added to the two single movements separately. For the first verification case, the magnetic disturbance was added only during the inclination movement; the shock disturbance was added only during the azimuth movement. For the second verification case, we reversed this and added the magnetic disturbance during the azimuth movement and the shock disturbance during the inclination movement.

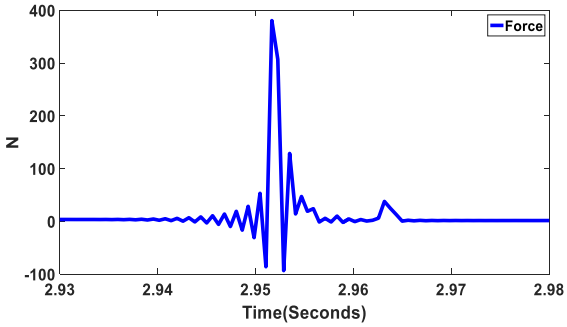

FIGURE 20. Shock force in verification case 2.

1) SENSITIVITY TO DISTURBANCE VERIFICATION CASE 1

For the first verification case (as shown in Figure 15), there were two movements: 90 degrees inclination (1st step) and 90 degrees azimuth (2nd step). First, the rotation arm was rotated from 0 degrees (vertical to the ground) to 90 degrees (horizontal) on the inclination plane. During this step, the

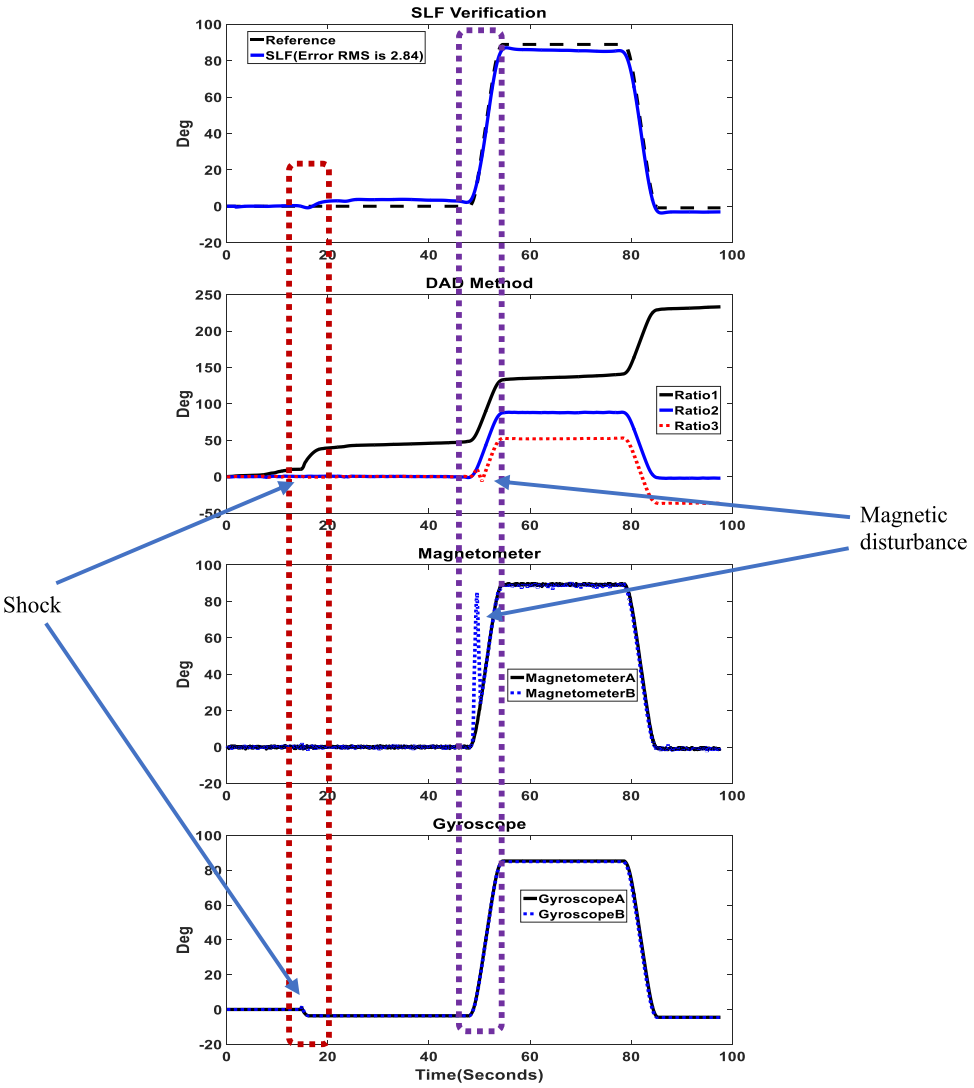

FIGURE 21. SLF performance in verification case 2.

azimuth angles were kept constant and only the inclination angles changed. In this inclination rotation, a magnetic disturbance was added to IMU_B. The magnetic disturbance (a magnet) was perpendicular to the inclination plane with a distance 0.3m from IMU_B. The magnetic disturbance caused a 40 degree deviation ($magnetometer_B$, Figure 17). The SLF reduced the deviation from 40 to 1.5 degrees as shown in subplot 1 of Figure 18.

After the first step finished, the rotation arm rotated around the rotation center of the horizontal plane from 0 degrees to 90 degrees then rotated back from 90 degrees to 0 degrees for the azimuth rotation. Also, a shock hammer was used to simulate a shock impact 0.15 m from IMU_A during this rotation. The hit direction was horizontal to the azimuth rotational plane and vertical to the rotational arm. Figure 16 shows the shock force delivered by a shock hammer (PCB 208. A03). The magnitude of the force was about 500N with only one impact. In verification case 1 without training, the SLF performance degraded from 0.259 to 2.227 (RMS value), and the maximum value of the error was 14 degrees.

2) SENSITIVITY TO DISTURBANCE VERIFICATION CASE 2

For the second verification case (Figure 19), there are two movements: 90 degrees inclination (1^{st} step) and 90 degrees azimuth (2^{nd} step). First, the rotation arm was rotated from 0 degrees (vertical) to 90 degrees (horizontal) on the inclination plane. During this step, the azimuth angles were kept constant and only the inclination angles changed. In this inclination rotation (1^{st} step), a shock hammer was used to deliver an impact 0.15 m from IMU_A in the azimuth rotation. The hit direction was parallel to the azimuth rotational plane and perpendicular to the inclination plane. After the first step finished, the rotation arm was only rotated around the rotation center of the horizontal plane from 0 degrees to 90 degrees (back and forth) for the azimuth rotation.

Also, a magnetic disturbance (applied using a magnet) was applied to IMU_B. The magnet was on the azimuth plane 0.3 m from IMU_B.

Figure 21 shows the results of the SLF azimuth estimation of verification case 2. The magnetic disturbance was implemented in the azimuth rotation and caused an 80 degrees deviation ($magnetometer_B$). In verification case 2 without training, the SLF performance degraded from 0.259 to 2.84 (RMS value) and the maximum value of the error was 5 degrees. The proposed SLF method performs less well in verification cases 2 compared to verification case 1, but both performed poorly compared to when training cases are used.

TABLE 3. The effect of the shock and magnetic disturbance in Case Study 1 (with training), Verification Case 1 and Verification Case 2 (without training).

	Case Study 1 (With training)		Verification Case 1 (Without training)		Verification Case 2 (Without training)	
Disturbances	Shock	Magnetic	Shock	Magnetic	Shock	Magnetic
MagnetometerA	O	O	O	O	O	O
MagnetometerB	O	×	O	×	O	×
GyroscopeA	×	O	×	O	×	O
GyroscopeB	×	O	×	O	×	O
DAD Ratio1	×	O	×	O	×	O
DAD Ratio2	×	O	×	O	×	O
DAD Ratio3	×	×	×	×	×	×
SLF	O	O	Δ	Δ	Δ	Δ

Table 3 illustrates the effect of shock and magnetic disturbances in case study 1 (with training) and verification case 1 and verification case 2 (without training). Symbol O represents the obtained results are not affected by disturbances, whereas symbol × represents the results are affected by the disturbances; and symbol **Δ** means the results obtained from SLF without training is greatly affected by disturbances compared to the SLF with training.

V. CONCLUSION AND FUTURE WORK

In this paper, we first used dual acceleration difference values to increase the redundant azimuth rotation information, similar to what gyroscopes provide, in cases that have no gyroscopes. However, direct applications of this set up cause large errors because of accelerometer noise and low robustness to shock impacts. To improve accuracy and robustness, we proposed using an SLF. All azimuth angles from magnetometers, gyroscopes, and accelerometers were compared, and their relative errors were put into the ANFIS to build error models. The final weights of each sensor were calculated according to the outputs of each error model.

The proposed method performs well under the assumed conditions: 1) the reference angle can be obtained, 2) only one magnetometer is affected by magnetic disturbances during a specific time interval because of distance D, 3) two IMUs rotate at one end of the rotation center, and 4) this method is only applied under similar conditions in a training environment. The unknown magnetic and shock disturbances caused angle errors that are corrected using the proposed fusion method. However, under the worst conditions (all sensors are not accurate), the error cannot be sufficiently reduced.

The proposed SLF was verified using two verification cases. In unknown application environments, without further training, the performance of SLF degraded from 0.259 (RMS error value) to 2.227 (RMS error value of verification case 1) and to 2.84 (RMS error value of verification case 2).

As future work, this research outcome can be extended to industry field applications. For example, the outcome can be combined with drilling survey data (used as a reference) to increase continuous wellbore positioning accuracy. The details of the drilling survey data obtained are shown in [1].

ACKNOWLEDGMENT

The authors wish to give special thanks to Dr. J. W. Kim at the University of Calgary for an introduction to drilling related geomatics.

REFERENCES

[1] H. Liu, R. Shor, and S. Park, "Intelligent wellbore path estimation using multiple integrated MEMS sensors," in *Proc. SPE/IADC Int. Drilling Conf. Exhib.*, The Hague, The Netherlands, 2019.
[2] A. Eldesoky, A. M. Kamel, M. Elhabiby, and H. Elhennawy, "Performance enhancement of low-cost MEMS inertial sensors using extensive calibration technique," in *Proc. 34th Nat. Radio Sci. Conf. (NRSC)*, Mar. 2017.
[3] Z.-J. Lu, Q. Xiang, and L. Xu, "An application case study on multi-sensor data fusion system for intelligent process monitoring," *Procedia CIRP*, vol. 17, pp. 721–725, Jan. 2014.
[4] J. Dong, D. Zhuang, Y. Huang, and J. Fu, "Advances in multi-sensor data fusion: Algorithms and applications," *Sensors*, vol. 9, no. 10, pp. 7771–7784, Sep. 2009.
[5] I. Aydin, S. B. Celebi, S. Barmada, and M. Tucci, "Fuzzy integral-based multi-sensor fusion for arc detection in the pantograph-catenary system," *Proc. Inst. Mech. Eng. F, J. Rail Rapid Transit*, vol. 232, no. 1, pp. 159–170, Jan. 2018.
[6] R. C. Luo and M. G. Kay, "Multisensor integration and fusion in intelligent systems," *IEEE Trans. Syst., Man, Cybern.*, vol. 19, no. 5, pp. 901–931, Sep. 1989.
[7] F. Cappello, S. Ramasamy, R. Sabatini, and J. Liu, "Low-cost sensors based multi-sensor data fusion techniques for RPAS Navigation and Guidance," in *Proc. Int. Conf. Unmanned Aircr. Syst. (ICUAS)*, Jun. 2015, pp. 714–722.
[8] B. Gao, G. Hu, S. Gao, Y. Zhong, and C. Gu, "Multi-sensor optimal data fusion based on the adaptive fading unscented Kalman filter," *Sensors*, vol. 18, no. 2, p. 488, Feb. 2018.
[9] B. Li, J. Lu, W. Xiao, and T. Lin, "In-field fast calibration of FOG-based MWD IMU for horizontal drilling," *Meas. Sci. Technol.*, vol. 26, no. 3, Mar. 2015, Art. no. 035001.
[10] M. ElGizawy, A. Noureldin, J. Georgy, U. Iqbal, and N. El-Sheimy, "Wellbore surveying while drilling based on Kalman filtering," *Amer. J. Eng. Appl. Sci.*, vol. 3, no. 2, pp. 240–259, Feb. 2010.
[11] X. Qilong, W. Ruihe, S. Feng, H. Leilei, and H. Laiju, "Continuous measurement-while-drilling utilizing strap-down multi-model surveying system," *IEEE Trans. Instrum. Meas.*, vol. 63, no. 3, pp. 650–657, Mar. 2014.
[12] C. Kao and T. Chen, "Design and analysis of an orientation estimation system using coplanar gyro-free inertial measurement unit and magnetic sensors," *Sens. Actuators A, Phys.*, vol. 144, no. 2, pp. 251–262, Jun. 2008.
[13] E. Bergamini, G. Ligorio, A. Summa, G. Vannozzi, A. Cappozzo, and A. Sabatini, "Estimating orientation using magnetic and inertial sensors and different sensor fusion approaches: Accuracy assessment in manual and locomotion tasks," *Sensors*, vol. 14, no. 10, pp. 18625–18649, Oct. 2014.
[14] B. Fan, Q. Li, and T. Liu, "How magnetic disturbance influences the attitude and heading in magnetic and inertial sensor-based orientation estimation," *Sensors*, vol. 18, no. 2, p. 76, Dec. 2017.

[15] R. Zhang and L. M. Reindl, "Pedestrian motion based inertial sensor fusion by a modified complementary separate-bias Kalman filter," in *Proc. IEEE Sensors Appl. Symp.*, Feb. 2011.

[16] C.-G. Lee, N.-N. Dao, S. Jang, D. Kim, Y. Kim, and S. Cho, "Gyro drift correction for an indirect Kalman filter based sensor fusion driver," *Sensors*, vol. 16, no. 6, p. 864, Jun. 2016.

[17] V. Larin and A. Tunik, "Gyro-free accelerometer-based SINS: Algorithms and structures," in *Proc. 2nd Int. Conf. 'Methods Syst. Navigat. Motion Control (MSNMC)*, Kiev, Ukraine, Oct. 2012, pp. 18–26.

[18] M. B. Bogdanov, A. A. Galkin, A. V. Prohortsov, V. V. Saveliev, and N. D. Udakova, "Integrated inertial/satellite orientation and navigation system on accelerometer-based SINS," in *Proc. 18th Saint-Petersburg Conf. Integr. Navigat. Syst.*, 2011, pp. 216–218.

[19] Y.-L. Tsai, T.-T. Tu, H. Bae, and P. H. Chou, "EcoIMU: A dual triaxial-accelerometer inertial measurement unit for wearable applications," in *Proc. Int. Conf. Body Sensor Netw.*, Jun. 2010.

[20] L. I. Iozan, M. Kirkko-Jaakkola, J. Collin, J. Takala, and C. Rusu, "Using a MEMS gyroscope to measure the Earth's rotation for gyro-compassing applications," *Meas. Sci. Technol.*, vol. 23, no. 2, Feb. 2012, Art. no. 025005.

[21] J. Cao, X. Zhu, H. Wu, and L. Zhang, "A novel method of measuring spatial rotation angle using MEMS tilt sensors," *Meas. Sci. Technol.*, vol. 28, no. 10, Oct. 2017, Art. no. 105907.

[22] J. Li, M. Broas, J. Makkonen, T. T. Mattila, J. Hokka, and M. Paulasto-Krockel, "Shock impact reliability and failure analysis of a three-axis MEMS gyroscope," *J. Microelectromech. Syst.*, vol. 23, no. 2, pp. 347–355, Apr. 2014.

[23] R. J. Shor, M. W. Dykstra, O. J. Hoffmann, and M. Coming, "For better or worse: Applications of the transfer matrix approach for analyzing axial and torsional vibration," in *Proc. SPE/IADC Drilling Conf. Exhib.*, 2015.

[24] M. Elgizawy, A. M. Noureldin, and N. El-Sheimy, "Continuous wellbore surveying while drilling utilizing MEMS gyroscopes based on Kalman filtering," in *Proc. SPE Annu. Tech. Conf. Exhibit.*, 2010.

[25] D. Gebre-Egziabher, R. Hayward, and J. Powell, "Design of multi-sensor attitude determination systems," *IEEE Trans. Aerosp. Electron. Syst.*, vol. 40, no. 2, pp. 627–649, Apr. 2004.

[26] X. Wang and C. Yang, "Constructing gyro-free inertial measurement unit from dual accelerometers for gesture detection," *Sensors Transducers*, vol. 171, no. 5, pp. 134–140, 2014.

[27] M. Z. H. Bhuiyan, H. Kuusniemi, L. Chen, L. Pei, L. Ruotsalainen, R. Guniness, and R. Chen, "Performance evaluation of multi-sensor fusion models in indoor navigation," *Eur. J. Navigat.*, vol. 11, no. 2, pp. 20–28, 2013.

[28] J.-O. Nilsson and I. Skog, "Inertial sensor arrays—A literature review," in *Proc. Eur. Navigat. Conf. (ENC)*, May 2016, p. 10.

[29] O. J. Woodman, "An introduction to inertial navigation," Comput. Lab., Univ. Cambridge., Cambridge, U.K., Tech. Rep. UCAM-CL-TR-696. [Online]. Available: http://www.cl.cam.ac.uk/techreports/

[30] P. Patonis, P. Patias, I. N. Tziavos, D. Rossikopoulos, and K. G. Margaritis, "A fusion method for combining low-cost IMU/magnetometer outputs for use in applications on mobile devices," *Sensors*, vol. 18, no. 8, p. 2616, Aug. 2018.

[31] G. De Pasquale and A. Somà, "Reliability testing procedure for MEMS IMUs applied to vibrating environments," *Sensors*, vol. 10, no. 1, pp. 456–474, Jan. 2010.

[32] K. Hemanth, V. Talasila, and S. Rao, "Calibration of 3-axis magnetometers," *IFAC Proc. Volumes*, vol. 45, no. 1, pp. 175–178, 2012.

[33] D. Yang, Z. You, B. Li, W. Duan, and B. Yuan, "Complete tri-axis magnetometer calibration with a gyro auxiliary," *Sensors*, vol. 17, no. 6, p. 1223, May 2017.

[34] Q. Ladetto, J. van Seeters, S. Sokolowski, Z. Sagan, and B. Merminod, "Digital magnetic compass and gyroscope for dismounted soldier position & navigation," *NATO Res. Technol. Agency, Sensors Electron. Technol. Panel, NATO Meetings*, 2002, p. 15.

[35] M. Denoual, K. Fodil, C. Dolabdjian, and F. Kauffmann, "Magnetic sensor noise impact on the evaluation of magnetorelaxometry experiments," in *Proc. 22nd Int. Conf. Noise Fluctuations (ICNF)*, Jun. 2013.

[36] M. Butta and I. Sasada, "Sources of noise in a magnetometer based on orthogonal fluxgate operated in fundamental mode," *IEEE Trans. Magn.*, vol. 48, no. 4, pp. 1508–1511, Apr. 2012.

[37] Kionix. (2008). *Using Two Tri-Axis Accelerometers for Rotational Measurements*. [Online]. Available: http://kionixfs.kionix.com/en/document/AN019.pdf

[38] Analog Device. *ADIS16448 Data Sheet*. Accessed: Feb. 2019. [Online]. Available: https://www.analog.com/media/en/technical-documentation/data-sheets/adis16448.pdf

[39] C. P. Gooneratne, B. Li, and T. E. Moellendick, "Downhole applications of magnetic sensor," *Sensors*, vol. 17, no. 10, p. 2384, 2017.

[40] S. T. Spantideas, S.-D.-J. Kakarakis, N. C. Kapsalis, and C. N. Capsalis, "Theoretical methods for studying distance and frequency scaling for AC magnetic fields in satellite missions," *IEEE Trans. Magn.*, vol. 52, no. 4, pp. 1–5, Apr. 2016.

[41] F. Wu, A. Vibhute, G. S. Soh, K. L. Wood, and S. Foong, "A compact magnetic field-based obstacle detection and avoidance system for miniature spherical robots," *Sensors*, vol. 17, no. 6, p. 1231, May 2017.

HUAN LIU received the Ph.D. degree in artificial systems science from Chiba University, Japan, and the second Ph.D. degree in subsurface sensing and machine learning from the University of Calgary, Canada. From 2006 to 2013, he was a Research Engineer with the Advanced Engineering Center of Isuzu Motors, Japan. Then, he joined the University of Waterloo, as a Research Fellow, until 2014. He is currently a Professional Engineer (P.Eng.) in Alberta, Canada. He is currently working with the Department of Geomatics Engineering, University of Calgary. His research has resulted in numbers of journal and conference publications, and eight granted patents. His current research interests include directional drilling, wellbore modeling and positioning, AI, machine learning, subsurface sensing, intelligent sensor fusion, MEMS, adaptive control and mechanical system modeling and simulation, robotics, and mechatronics.

ROMAN J. SHOR received the B.A. degree in mathematics and the B.S.E. and M.S.E. degrees in computer science from the University of Pennsylvania, and the M.S.E. and Ph.D. degree in petroleum engineering from The University of Texas at Austin. He is currently an Assistant Professor with the Department of Chemical and Petroleum Engineering, Schulich School of Engineering, University of Calgary. His research interests include the areas of drill string dynamics modeling and control, drilling optimization, and drilling systems automation. Specifically, the application of reduced order modeling and modeling for control to enable model predictive control for drilling tasks and drilling optimization through data processing and machine learning. He is also interested in reducing the impact of drilling operations on the environment and surrounding communities. His collaborative research projects include an investigation of fluid rheology with applications to drilling fluids, magnetorheological fluids and their applications, hydraulic fracture placement optimization and applications of seismic processing methods to drillstring imaging. Finally, he is also active in the areas of machine learning and artificial intelligence with particular attention to applications in oil and gas.

SIMON S. PARK received bachelor's and master's degrees from the University of Toronto, Canada, and the Ph.D. from the University of British Columbia, Canada. He is currently a Professor with the Department of Mechanical and Manufacturing Engineering, Schulich School of Engineering, University of Calgary. He was an AITF iCORE Chair in sensing and monitoring. He is also a Professional Engineer in Alberta, and an Associate Member of CIRP (Int. Academy of Production Engineers) from Canada. He has worked in several companies, including IBM manufacturing, where he was a procurement engineer for printed circuit boards and Mass Prototyping Inc., dealing with rapid prototyping systems.